Relationship of the elastic and nonlinear acoustic properties of the antiferromagnetic fcc $Fe_{60}Mn_{40}$ single-crystal alloy to Invar behavior

M. Cankurtaran,* G. A. Saunders, P. Ray, and Q. Wang
School of Physics, University of Bath, Bath BA27AY, United Kingdom

U. Kawald, J. Pelzl, and H. Bach
Institut für Experimentalphysik, Ruhr-Universität Bochum, Germany
(Received 23 April 1992; revised manuscript received 15 October 1992)

The elastic and nonlinear acoustic properties of an antiferromagnetic fcc iron-manganese alloy single crystal with composition 60 at. % Fe have been studied with the ultrasonic pulse-echo-overlap technique. Velocity measurements of the three ultrasonic modes that can be propagated along the [110] direction have been made between 4.2 and 750 K to obtain all three independent elastic-stiffness-tensor components C_{IJ} and the adiabatic bulk modulus B^S as a function of temperature. At 293 K the elastic stiffnesses are $C_{11}=170$ GPa, $C_{12}=98$ GPa, and $C_{44}=142$ GPa; hence C_{11} and $B^S=123$ GPa are small, conforming with recognized trends for $3d$ transition-metal alloys. The Néel temperature T_N, assessed from electrical-resistance measurements and the steplike decrease in the temperature dependence of the shear modulus $(C_{11}-C_{12})/2$, is 467 K. The contributions of antiferromagnetic ordering to $C_L[=(C_{11}+C_{12}+2C_{44})/2]$, $(C_{11}-C_{12})/2$, and B^S are negative for all temperatures, while C_{44} is stiffened slightly. Measurements of the hydrostatic pressure dependences of the velocities of ultrasonic modes propagated along the [110] direction have been used to obtain the hydrostatic pressure derivatives $(\partial C_{IJ}/\partial P)_{P=0}$ of the elastic-stiffness-tensor components as a function of temperature in the antiferromagnetic Invar state. At 293 K, $(\partial C_{11}/\partial P)_{P=0}$, $(\partial C_{12}/\partial P)_{P=0}$, $(\partial C_{44}/\partial P)_{P=0}$, and $(\partial B^S/\partial P)_{P=0}$ are 10.1 ± 0.2, 7.1 ± 0.2, 3.84 ± 0.06, and 8.1 ± 0.2, respectively. To establish the vibrational anharmonicity of the long-wavelength acoustic modes, the results obtained for the C_{IJ} and $(\partial C_{IJ}/\partial P)_{P=0}$ have been used to calculate the corresponding Grüneisen parameters. The observation that at 293 K the mean long-wavelength acoustic-mode Grüneisen parameter $\bar{\gamma}^{el}(=2.12)$ is much larger than the thermal Grüneisen parameter $\gamma^{th}(=0.81)$ shows that the vibrational anharmonicities of the long-wavelength acoustic modes are, on average, substantially larger than those of phonons having larger wave vectors. Magnetoelastic contributions to the vibrational anharmonicity of the long-wavelength acoustic modes of antiferromagnetic $Fe_{60}Mn_{40}$ and ferromagnetic $Fe_{72}Pt_{28}$ and $Fe_{65}Ni_{35}$ Invar alloys are discussed in relation to the recently developed theoretical explanation of the behavior of Invar alloys based on fixed-spin-moment calculations of the total energy for low-spin and high-spin configurations.

I. INTRODUCTION

The Fe-Mn alloys are stable in the fcc (γ) phase in the composition range between about 40 and 70 at. % Fe.[1,2] No ordering between the Fe and Mn atoms has been detected at any composition.[3] The γ Fe-Mn alloys are antiferromagnetic and their magnetic properties have been interpreted by an itinerant electron model. These alloys show Invar effects.[4–8] Although the thermal expansion of $Fe_{60}Mn_{40}$ shows characteristic Invar-type behavior between about 200 and 450 K, it is much less pronounced than that of the ferromagnetic Invar alloys $Fe_{72}Pt_{28}$ and $Fe_{65}Ni_{35}$, which occur in much the same temperature range (Fig. 1). The spontaneous volume magnetostriction is positive, reaching about 50% that of $Fe_{65}Ni_{35}$.[9] Application of pressure reduces the Néel temperature T_N of $Fe_{70}Mn_{30}$ by -25 K/GPa.[4]

The Invar anomalies are observed for ferromagnetic (FM) alloys having about 8.5 electrons per atom (e/a) and antiferromagnetic (AFM) alloys with e/a about 7.5.[10,11] Magnetovolume instabilities have important ramifications in the elastic properties of Invars, prompting this ultrasonic study of the effects of temperature and hydrostatic pressure on the elastic behavior of monocrystalline antiferromagnetic $Fe_{60}Mn_{40}$. Previously the elastic moduli of Fe-Mn alloys of similar composition have been measured above room temperature up to 600 K.[12,13] To enable a more accurate assessment of the contribution of AFM ordering to the elastic stiffnesses, the temperature range of elastic moduli measurements has now been extended both to higher temperatures up to 750 K in the paramagnetic state and down from room temperature to liquid-helium temperatures. To establish the nonlinear acoustic properties in the antiferromagnetic phase, the ultrasonic wave velocities have been measured as a function of hydrostatic pressure up to 0.15 GPa in the temperature range between 293 and 453 K.

Recently, Mañosa *et al.*[14,15] discovered for the Invar ferromagnetic alloy $Fe_{72}Pt_{28}$ that the velocities of all the longitudinal and quasilongitudinal ultrasonic modes decrease under hydrostatic pressure. The pressure derivatives $(\partial C_{11}/\partial P)_{P=0}$ and $(\partial C_L/\partial P)_{P=0}$ (where $C_L[=(C_{11}+C_{12}+2C_{44})/2]$) of the longitudinal-mode elastic stiffnesses are negative in the ferromagnetic phase

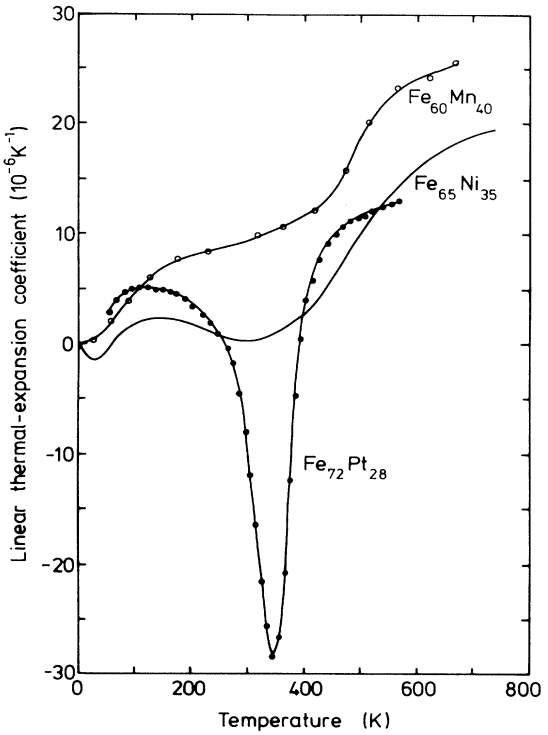

FIG. 1. The linear thermal expansion coefficient as a function of temperature for the $Fe_{60}Mn_{40}$ alloy (Ref. 7) in comparison with those of disordered $Fe_{72}Pt_{28}$ (Ref. 16) and $Fe_{65}Ni_{35}$ (Ref. 6).

of $Fe_{72}Pt_{28}$, while being positive in the paramagnetic phase. Hence the long-wavelength longitudinal acoustic modes have negative Grüneisen parameters accounting for the negative thermal expansion (Fig. 1) observed[16] in $Fe_{72}Pt_{28}$ in the temperature range between about 260 and 390 K: soft longitudinal acoustic modes play an important role in the Invar behavior of ferromagnetic $Fe_{72}Pt_{28}$. One aim of the present study has been to establish the magnitude of the contribution from the anharmonicity of long-wavelength acoustic phonons to Invar effects in an antiferromagnetic alloy. The experimental results for $Fe_{60}Mn_{40}$ are compared with those reported previously for the typical ferromagnetic Invars $Fe_{72}Pt_{28}$ (Refs. 14 and 15) and $Fe_{65}Ni_{35}$,[13] which are now explained in the framework of developments in understanding of Invar behavior in ferromagnetic alloys.[17–19]

II. EXPERIMENTAL PROCEDURE

A single crystal of cm^3 dimensions was grown from high-purity elements by a modified Bridgman process.[20] The alloy charge was contained in an alumina crucible; since the vapor pressure of molten manganese is high, the crucible with the charge was sealed in a molybdenum container. The crystal was large enough for precision measurements of ultrasonic wave velocities and their temperature and pressure dependences. Microprobe analysis scans around the crystal showed its composition to be $Fe_{60}Mn_{40}$ within ± 1 at. %. The lattice parameter was determined from x-ray powder analysis as 3.614 ± 0.001 Å. The x-ray density was 7820 ± 30 kg m^{-3}. The crystal was orientated on a three-arc goniometer to $\pm 0.5°$ using Laue back-reflection photography. An ultrasonic sample was cut and polished with two faces, normal to the required propagation direction along the [110] crystallographic axis, flat to surface irregularities of about 2 μm and parallel to better than 10^{-3} rad. The Néel temperature of the sample was determined from electrical resistance (R) measurements, as the start temperature of the anomaly in the derivative $(1/R_0)(dR/dT)$, following the approach used by Bendick and Pepperhoff.[21] The result obtained for T_N (=467 K) is in agreement with that (468 K) determined from magnetic susceptibility measurements.[22]

Ultrasonic wave velocity measurements were made along the [110] direction. 10-MHz ultrasonic pulses were generated and detected by X- and Y-cut quartz transducers bonded to the sample using Apiezon N for low-temperature experiments or Krautkrämer ZGM high-temperature coupling paste above 300 K. Dow resin was used as bonding material for high-pressure experiments. Ultrasonic pulse transit times were measured using a pulse-echo-overlap technique[23] capable of resolution of velocity changes to 1 part in 10^5 and particularly well suited to determination of pressure or temperature-induced changes in velocity. The temperature dependence of ultrasound velocity was measured between 4.2 and 750 K. Hydrostatic pressure up to 0.15 GPa was applied in a piston and cylinder apparatus sealed with Teflon and Viton O rings. Silicon fluid was used as the pressure transmitting medium. The dependence of ultrasonic wave velocity upon hydrostatic pressure was measured between 293 and 453 K. Temperatures above room temperature were reached within the pressure cell by using a heating element wrapped round the outside of the pressure cylinder. During pressure runs it was essential to ensure that velocity measurements were made at the same controlled temperature within 0.2 °C. The pressure was measured using the change in resistance of a precalibrated manganin wire coil inside the cell. For further details of the experimental setup see Flower and Saunders.[24] To bypass calculation of the changes in crystal dimensions induced by application of hydrostatic pressure, the experimental data were transformed to correspond to the "natural velocity" W.[25] Then an iterative procedure of the type introduced by Dandekar[26] was used to improve the accuracy of determination of the elastic-stiffness-tensor components and their hydrostatic pressure derivatives as a function of temperature. The major sources of error in decreasing order of magnitude were in the measurement of pressure, alloy composition, sample dimensions, and alignment.

III. THE ELASTIC-STIFFNESS-TENSOR COMPONENTS AND THEIR DEPENDENCES UPON TEMPERATURE

The adiabatic elastic-stiffness-tensor components of $Fe_{60}Mn_{40}$ measured at room temperature (Table I) are in reasonable agreement with the results obtained for an al-

TABLE I. Comparison between the room-temperature (293 K) elastic and nonlinear acoustic properties of the $Fe_{60}Mn_{40}$ alloy and those of other Invars ($Fe_{65}Ni_{35}$ and $Fe_{72}Pt_{28}$) and the elements Fe and Ni.

Description	Ni (Ref. 27)	Fe (Ref. 27)	$Fe_{60}Mn_{40}$	$Fe_{65}Ni_{35}$ (Ref. 15)	$Fe_{72}Pt_{28}$ (Ref. 15)
Density ($kg\,m^{-3}$)	8 900	7 873	7 820	8 121	11 939
Elastic stiffnesses (10 GPa)					
C_{11}	24.7	23.0	17.0±0.1	13.6±0.1	14.4±0.1
C_{44}	12.2	11.7	14.1±0.1	9.8±0.1	8.0±0.1
C_{12}	15.3	13.5	9.8±0.2	9.2±0.2	10.7±0.2
$\frac{1}{2}(C_{11}-C_{12})$	4.7	4.7	3.6±0.1	2.2±0.1	1.8±0.1
Bulk modulus B^S (10 GPa)	18.4	16.7	12.3±0.2	10.7±0.2	12.0±0.2
Pressure derivatives					
$(\partial C_{11}/\partial P)_{P=0}$	6.0	6.7	10.1	5.2	−19.2
$(\partial C_{12}/\partial P)_{P=0}$	4.7	4.6	7.1	−2.1	−26
$(\partial C_{44}/\partial P)_{P=0}$	2.4	2.6	3.8	5.7	0.6
$(\partial C'/\partial P)_{P=0}$	0.6	1.0	1.5	3.6	−18
$(\partial B^S/\partial P)_{P=0}$	5.3	5.3	8.1	0.3	−23.7

loy of the same nominal composition[13] and those for $Fe_{61}Mn_{39}$.[12] Comparison shows that the elastic moduli C_{11} and C_L of iron-based Invar alloys are substantially smaller than those for the transition elements iron and nickel (Table I): their long-wavelength longitudinal phonons are softer. Lenkkeri[28] noted that the elastic moduli of fcc transition-metal alloys are strongly dependent on the e/a ratio. The bulk modulus of $Fe_{60}Mn_{40}$, for which the e/a ratios is 7.6, conforms with the trend found by Lenkkeri for alloys with an e/a ratio in this vicinity.

The temperature dependences of the adiabatic elastic stiffnesses C_L, C_{44}, and $C'[=(C_{11}-C_{12})/2]$ and the bulk modulus $B^S(=C_L-C_{44}-C'/3)$ in both the antiferromagnetic and paramagnetic states of $Fe_{60}Mn_{40}$ are shown in Fig. 2. Corrections for lengths and density changes with temperature have been made using the thermal expansion data.[7] This set of elastic-stiffness data up to, through, and well above the Néel temperature complements and extends to a much wider range of temperature the data for C_{44}, $(C_{11}-C_{12})/2$, and B^S measured[13] between 293 and 593 K for an alloy of the same nominal composition. In the paramagnetic range, for temperatures well above 575 K, the elastic stiffnesses and the bulk modulus decrease approximately linearly with increasing temperature. In the vicinity of the antiferromagnetic transition, C_L, C', and B^S soften. The longitudinal modulus C_L shows a small dip [Fig. 2(a)]. The shear modulus C' exhibits the largest change as the temperature is lowered through T_N showing a steplike reduction at 467 K of about 3.8% [Fig. 2(c)], while C_{44} shows only a small change in gradient near this point [Fig. 2(b)]. Renaud[13] reported a steplike decrease of about 9% in the value of C' at 463 K. Lenkkeri[12] who measured the elastic moduli C_L, C_{44}, and $(C_{11}-C_{12})/2$ for $Fe_{61}Mn_{39}$ between 300 and 600 K also found a similar steplike decrease in the shear modulus $(C_{11}-C_{12})/2$.

An estimate of the magnetic contribution to the elastic stiffnesses can be made by using the procedure, employed[29] for antiferromagnetic Mn-Ni alloys, of extrapolating the data obtained in the paramagnetic state down below T_N. To do this, the temperature dependence of each elastic stiffness in the paramagnetic state has been approximated by the conventional model for vibrational anharmonicity using[30]

$$C=C_0[1-KF(T/\Theta_D)] \tag{1}$$

with

$$F(T/\Theta_D)=3(T/\Theta_D)^4\int_0^{\Theta_D/T}\frac{x^3dx}{e^x-1}. \tag{2}$$

The constants C_0 and K have been chosen to fit the elastic stiffness data in the paramagnetic phase above 600 K; the Debye temperature Θ_D is 410 K obtained[31] from specific-heat measurements for $Fe_{60}Mn_{40}$. The extrapolated elastic stiffnesses obtained using Eqs. (1) and (2) are shown by dashed lines in Fig. 2. A precursive effect, consistent with onset of short-range antiferromagnetic ordering, on the elastic stiffnesses starts to appear at about 575 K—well above the Néel temperature (Fig. 2). The magnetic contributions to C_L, C', and B^S are negative for all temperatures: in the antiferromagnetic state C_L, C', and B^S are softened, while C_{44} is stiffened slightly. At 4.2 K the contribution from the antiferromagnetic ordering reduces $(C_{11}-C_{12})/2$, C_L, and B^S by about 27, 4.6, and 8.8%, respectively, while increasing C_{44} by about 1%. These changes in the values of the elastic stiffnesses define the magnitudes of the magnetoelastic interactions. Renaud[13] reported a negative magnetic contribution to $(C_{11}-C_{12})/2$ and a positive one to C_{44} in the antiferromagnetic range; the contribution to B^S was negative in the vicinity of T_N but positive for temperatures below about 400 K. However, his measurements only cover the temperature range between 293 and 593 K; this is also the case in Lenkkeri's work.[12] Since the influence of the antiferromagnetic phase transition on the elastic moduli already starts at about 575 K, these researchers could not extrapolate the high-temperature behavior correctly.

The ultrasonic wave velocity measurements show no indications of a crystallographic phase transition in the

temperature range from 750 down to 4.2 K. The shear stiffness $(C_{11}-C_{12})/2$ in both the paramagnetic and antiferromagnetic states of $Fe_{60}Mn_{40}$ follows the normal tendency to increase as the temperature is decreased [Fig. 2(c)] in marked distinction to the behavior of $(C_{11}-C_{12})/2$ for the fcc Mn-Ni, Fe-Ni, and Fe-Pt alloys.[32,33,15] Although $(C_{11}-C_{12})/2$ is somewhat reduced as $Fe_{60}Mn_{40}$ is taken down in temperature through T_N, the softening of this shear modulus is not large enough to induce the lattice instability that results in the ferroelastic fcc-fct transitions associated with shear in a $\langle 1\bar{1}0\rangle$ direction on a $\langle 110\rangle$ plane.

IV. THE HYDROSTATIC PRESSURE DERIVATIVES OF THE ELASTIC-STIFFNESS-TENSOR COMPONENTS AND THE COMPRESSION OF $Fe_{60}Mn_{40}$

The velocities of the three ultrasonic modes propagated along the [110] direction increase linearly with pressure, more steeply for the longitudinal than the shear modes. The experimental results obtained for the hydrostatic pressure derivatives $(\partial C_L/\partial P)_{P=0}$, $(\partial C_{44}/\partial P)_{P=0}$, $(\partial C'/\partial P)_{P=0}$, and $(\partial B^S/\partial P)_{P=0}$ of the adiabatic second-order elastic stiffness and the bulk modulus, at selected temperatures between 293 and 453 K, are given in Table II. All of these quantities are positive and decrease as the temperature is increased up towards T_N.

The temperature dependences of $(\partial C_L/\partial P)_{P=0}$ and $(\partial B^S/\partial P)_{P=0}$ for $Fe_{60}Mn_{40}$ are compared with those of the ferromagnetic $Fe_{72}Pt_{28}$ (Ref. 15) and $Fe_{65}Ni_{35}$ (Ref. 13) Invar alloys in Fig. 3. It is clear that, as a consequence of the magnetovolume effect, there is a close correlation between the magnitudes of the Invar anomaly in the thermal expansion (Fig. 1) and the pressure derivative of the elastic stiffness of the longitudinal acoustic mode and that of the bulk modulus (Fig. 3). In the Invar region, $Fe_{72}Pt_{28}$ has large negative values of thermal expansion,[16] $(\partial C_L/\partial P)_{P=0}$ and $(\partial B^S/\partial P)_{P=0}$.[14,15] This is extraordinary: on warming $Fe_{72}Pt_{28}$ shrinks, under compression it becomes easier to squeeze. The large neg-

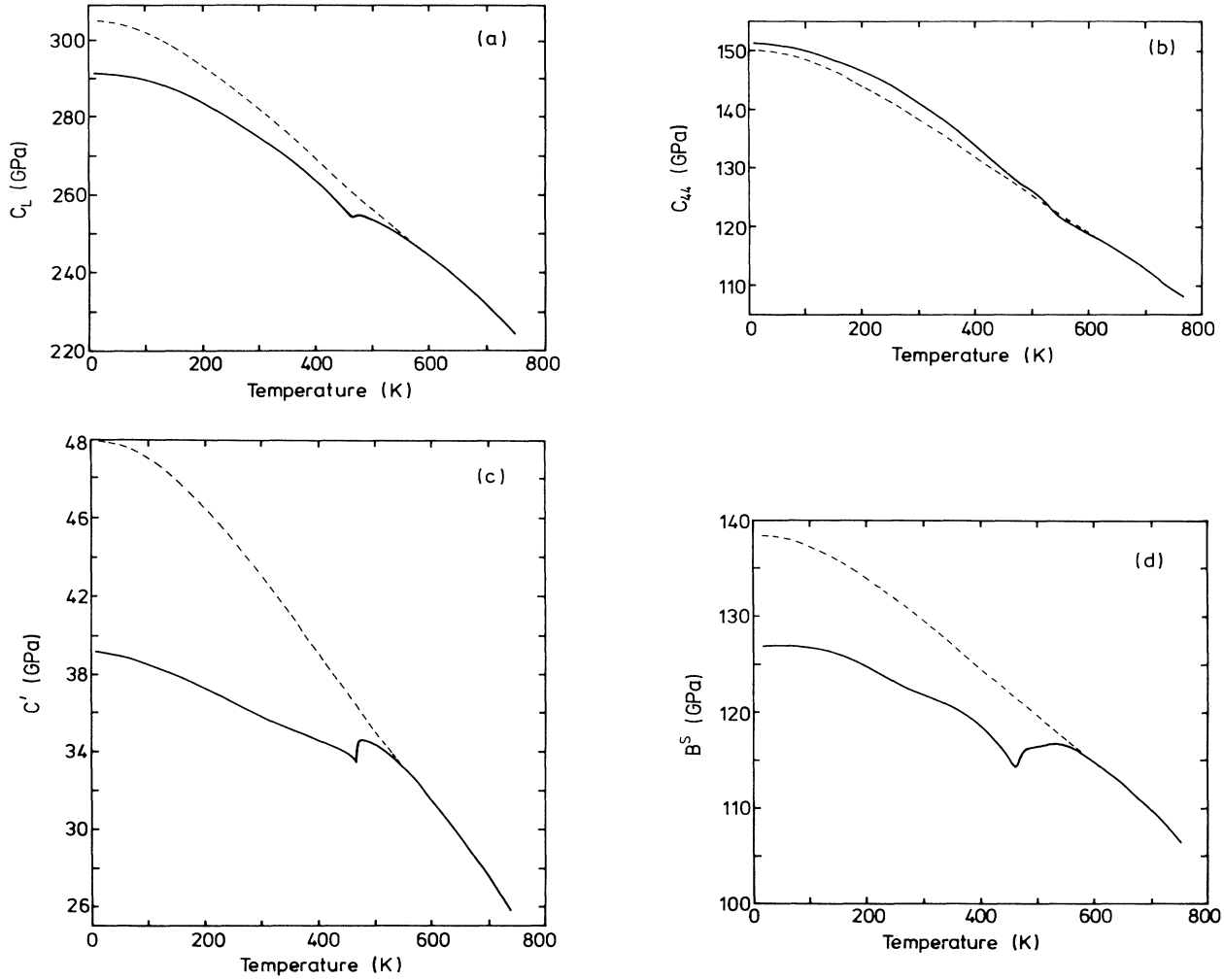

FIG. 2. The temperature dependences of the elastic stiffness (a) $C_L[=(C_{11}+C_{12}+2C_{44})/2]$, (b) C_{44}, (c) $C'[=(C_{11}-C_{12})/2]$, and (d) the bulk modulus of B^S of the monocrystalline $Fe_{60}Mn_{40}$ alloy. The solid line shows the experimental results and the dashed line corresponds to extrapolated values obtained using Eqs. (1) and (2).

TABLE II. The temperature dependences of the hydrostatic pressure derivatives $(\partial C_L/\partial P)_{P=0}$, $(\partial C_{44}/\partial P)_{P=0}$, $(\partial C'/\partial P)_{P=0}$, and $(\partial B^S/\partial P)_{P=0}$ for $Fe_{60}Mn_{40}$ Invar alloy crystal.

T (K)	$(\partial C_L/\partial P)_{P=0}$	$(\partial C_{44}/\partial P)_{P=0}$	$(\partial C'/\partial P)_{P=0}$	$(\partial B^S/\partial P)_{P=0}$
293	12.45±0.2	3.84±0.06	1.46±0.05	8.12±0.1
313	10.99±0.2	3.72±0.09	1.57±0.04	6.75±0.1
333	8.69±0.2	2.72±0.05	0.53±0.01	5.80±0.1
353	7.78±0.2	1.18±0.1	0.41±0.01	6.47±0.1
373	7.96±0.2	2.68±0.1	0.37±0.01	5.16±0.1
393	7.23±0.2			
413	7.46±0.2			
428	6.22±0.2			
453	6.99±0.2			

ative $(\partial B^S/\partial P)_{P=0}$ relates directly to the negative thermal expansion: both properties involve the cubic term in the strain energy of the identical irreducible representation η_0^0, which is the volume strain $(\eta_{11}+\eta_{22}+\eta_{33})$. In the case of the classic Invar material $Fe_{65}Ni_{35}$ there is a pause in the thermal expansion (Fig. 1) coupled with an almost zero value of $(\partial B^S/\partial P)_{P=0}$ in the same temperature interval (Table I, Fig. 3). The Invar anomaly in the thermal expansion for the antiferromagnetic $Fe_{60}Mn_{40}$ is much weaker and, consequently, $(\partial B^S/\partial P)_{P=0}$ is positive (Table II).

Measurements of the elastic stiffness and their hydrostatic pressure dependences can be used to evaluate the compression $V(P)/V_0$ up to very high pressures, using an extrapolation procedure based on the Murnaghan equation of state in the logarithmic form

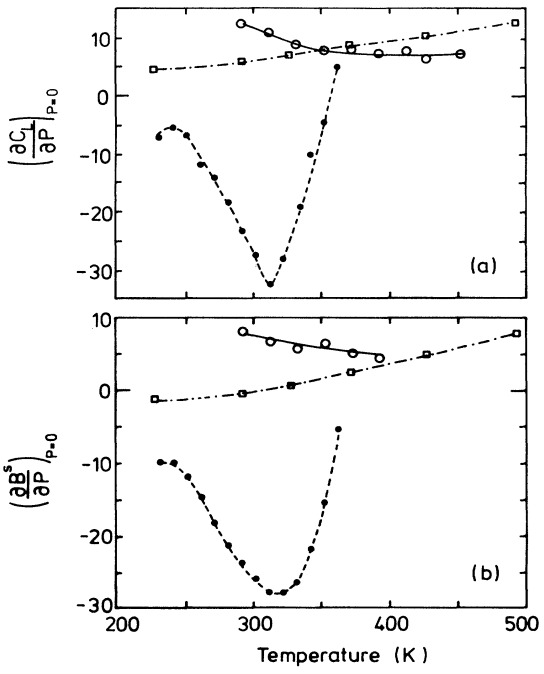

FIG. 3. The temperature dependences of hydrostatic pressure derivatives (a) $(\partial C_L/\partial P)_{P=0}$ of the longitudinal elastic stiffness and (b) $(\partial B^S/\partial P)_{P=0}$ of the bulk modulus for $Fe_{60}Mn_{40}$ (open circles), $Fe_{72}Pt_{28}$ (solid circles) (Ref. 15), and $Fe_{65}Ni_{35}$ (open squares) (Ref. 13). The lines are for visual guidance.

$$\ln\left[\frac{V_0}{V(P)}\right]=\frac{1}{B_0'^T}\ln\left[B_0'^T\left[\frac{P}{B_0^T}\right]+1\right], \tag{3}$$

which describes the compression of many solids well.[34] Ultrasonic measurements provide adiabatic (S) elastic moduli, so to use this equation of state it is necessary to transform the input data to isothermal (T) moduli. The adiabatic and isothermal bulk moduli are related by

$$B^S=B^T(1+\alpha\gamma^{\rm th}T), \tag{4}$$

where α is the coefficient of volume expansion. The isothermal bulk modulus B^T at 293 K has been determined as 121.5 GPa taking $\alpha=26.4\times10^{-6}$ K^{-1} (Ref. 7) and $\gamma^{\rm th}=0.81$ (see Sec. V). The hydrostatic pressure derivative B'^T $[=(\partial B^T/\partial P)_{P=0}]$ has been calculated using[34,35]

$$B'^T=B'^S+T\alpha\gamma^{\rm th}\left[\frac{B^T}{B^S}\right]\left[1-\frac{2}{\alpha B^T}\left[\frac{\partial B^T}{\partial T}\right]_P-2B'^S\right]+\left[T\alpha\gamma^{\rm th}\left[\frac{B^T}{B^S}\right]\right]^2\left[B'^S-1-\frac{1}{\alpha^2}\left[\frac{\partial\alpha}{\partial T}\right]_P\right], \tag{5}$$

where $(\partial B^T/\partial T)_P$ is given by

$$\left[\frac{\partial B^T}{\partial T}\right]_P=\left[\frac{\partial B^S}{\partial T}\right]\Big/(1+T\alpha\gamma^{\rm th})-\frac{B^S}{T}\frac{T\alpha\gamma^{\rm th}}{[1+T\alpha\gamma^{\rm th}]^2}\left\{1+\frac{(\partial\alpha/\partial T)_P}{\alpha/T}\right\}. \tag{6}$$

All quantities in Eqs. (4)–(6) are taken in the limit of zero pressure. A value of -2.94×10^7 Pa K^{-1} for the derivative of adiabatic bulk modulus with respect to temperature $(\partial B^S/\partial T)$ at 293 K has been obtained from the data in Fig. 2(d). The value of $(\partial\alpha/\partial T)(=1.38\times10^{-8}$ K$^{-2})$ has been deduced from the data given in Ref. 7. Insertion of data for B^S, $(\partial B^S/\partial T)$, α, $\gamma^{\rm th}$, and $(\partial\alpha/\partial T)$ into Eq. (6) gives a value of -3.21×10^7 Pa K^{-1} for $(\partial B^T/\partial T)$ at 293 K and then, from Eq. (5), $(\partial B^T/\partial P)_{P=0}$ has been calculated at 8.15. The compression of $Fe_{60}Mn_{40}$ at room temperature is compared with that of Ni in Fig. 4; in accord with its Invar behavior $Fe_{60}Mn_{40}$ has a much larger compression than Ni.

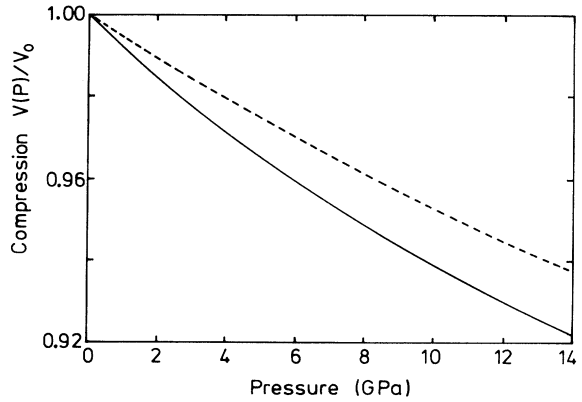

FIG. 4. The isothermal compression of $Fe_{60}Mn_{40}$ (solid line), extrapolated to very high pressures by using the Murnaghan equation of state, compared with that of Ni (dashed line).

V. GRÜNEISEN PARAMETERS AND ACOUSTIC-MODE VIBRATIONAL ANHARMONICITY OF $Fe_{60}Mn_{40}$ AND $Fe_{72}Pt_{28}$ INVAR ALLOYS

Both the pressure dependence of second-order elastic-stiffness moduli and the thermal expansion are consequences of the anharmonicity of lattice vibrations. However, while the nonlinear acoustic properties arise solely from the acoustic modes in the long-wavelength limit, the thermal expansion includes contributions from phonons of wave vectors spanning the entire Brillouin zone in all branches. In the quasiharmonic approximation the thermal Grüneisen parameter $\gamma^{\rm th}$ is the weighted average of all the individual excited mode Grüneisen parameters $\gamma_i(=-\partial \ln\omega_i/\partial \ln V)$ and is given by

$$\gamma^{\rm th}=\sum_i C_i\gamma_i \Big/ \sum_i C_i=\alpha VB^S/C_p=\alpha VB^T/C_V, \tag{7}$$

where C_i represents the Einstein heat capacity associated with mode i and reflects the contribution of this mode to $\gamma^{\rm th}$, V is the molar volume, C_P and C_V are specific heat at constant pressure and constant volume, respectively. The temperature dependence between 100 and 620 K of $\gamma^{\rm th}$ (Fig. 5) has been determined using thermal expansion[7] and heat capacity[31] data and the bulk modulus B^S given in Fig. 2(d). $\gamma^{\rm th}$ is positive; below about 200 K it is almost constant, in the Invar region it decreases slightly and then above the Néel temperature it increases quite steeply, following the behavior of the thermal expansion with temperature (Fig. 1).

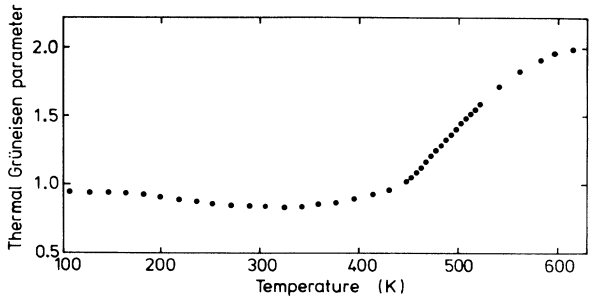

FIG. 5. The temperature dependence of the thermal Grüneisen parameter $\gamma^{\rm th}$ of the $Fe_{60}Mn_{40}$ alloy single crystal.

The pressure derivatives $(\partial C_{IJ}/\partial P)_{P=0}$ of the elastic stiffness can be used to determine the Grüneisen parameters for acoustic modes adjacent to the Brillouin zone center and hence resolve the role of such modes in the Invar behavior. For a cubic crystal the acoustic mode Grüneisen parameter can be calculated using[36]

$$\gamma_p(\mathbf{N})=-\frac{1}{6w_p(\mathbf{N})}[3B^T+2w_p(\mathbf{N})+k_p(\mathbf{N})], \tag{8}$$

where

$$w_p(\mathbf{N})=C_{11}^S k_1(p,\mathbf{N})+C_{44}^S k_2(p,\mathbf{N})+C_{12}^S k_3(p,\mathbf{N}), \tag{9}$$

and

$$\begin{aligned} k_p(\mathbf{N})=&-k_1(p,\mathbf{N})\left[C_{11}^S+3B^T+3B^T\left[\frac{\partial C_{11}^S}{\partial P}\right]_T\right] \\ &-k_2(p,\mathbf{N})\left[C_{44}^S+3B^T+3B^T\left[\frac{\partial C_{44}^S}{\partial P}\right]_T\right] \\ &-k_3(p,\mathbf{N})\left[C_{12}^S-3B^T+3B^T\left[\frac{\partial C_{12}^S}{\partial P}\right]_T\right], \end{aligned} \tag{10}$$

with

$$\begin{aligned} k_1(p,\mathbf{N})&=N_1^2U_1^2+N_2^2U_2^2+N_3^2U_3^2, \\ k_2(p,\mathbf{N})&=(N_2U_3+N_3U_2)^2+(N_3U_1+N_1U_3)^2 \\ &\quad+(N_1U_2+N_2U_1)^2, \\ k_3(p,\mathbf{N})&=2(N_2N_3U_2U_3+N_3N_1U_3U_1+N_1N_2U_1U_2). \end{aligned} \tag{11}$$

Here p (=1,2,3) designates the acoustic-mode branch, $\mathbf{q}$ is the wave vector, ω is the angular frequency of lattice vibrations, and N_i and U_i $(i=1,2,3)$ are the direction cosines of the wave propagation and the particle displacement directions, respectively. The acoustic-mode Grüneisen parameters in the long-wavelength limit, at room temperature (293 K) and 373 K, are shown in Fig. 6 as a function of propagation direction. All modes have a positive $\gamma_p(\mathbf{N})$; this property of $Fe_{60}Mn_{40}$ is in marked contrast to that of $Fe_{72}Pt_{28}$ for which the longitudinal-mode Grüneisen parameters are large and negative in the ferromagnetic phase.

The mean long-wavelength acoustic Grüneisen parameter $\bar{\gamma}^{\rm el}$ has been obtained by summing all of the long-wavelength acoustic-mode Grüneisen parameters with the same weight for each mode:

$$\bar{\gamma}^{\rm el}=\frac{\sum_{p=1}^{3}\int_\Omega \gamma_p(\mathbf{N})d\Omega}{3\int_\Omega d\Omega}. \tag{12}$$

Here the integration is over the whole space Ω. At 293 K, $\bar{\gamma}^{\rm el}$ (=2.12) is much larger than the corresponding thermal Grüneisen parameter $\gamma^{\rm th}$ (=0.81). This result shows that, in the Invar region, the vibrational anhar-

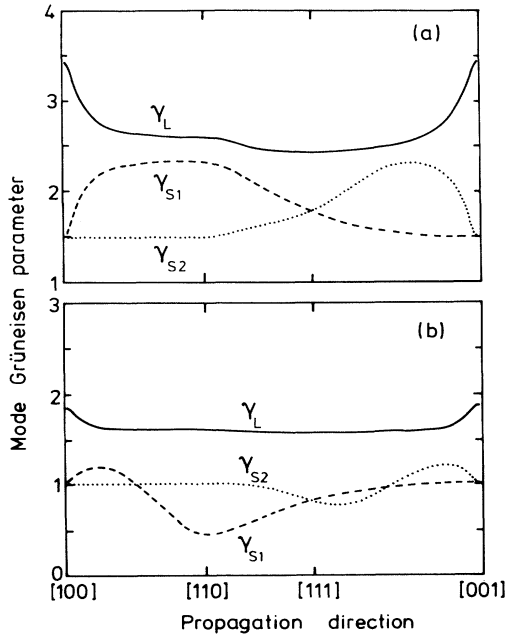

FIG. 6. Long-wavelength, longitudinal (solid line) and shear (dashed and dotted lines) acoustic-mode Grüneisen parameters of monocrystalline $Fe_{60}Mn_{40}$ alloy as a function of mode propagation direction at (a) 293 K and (b) 373 K.

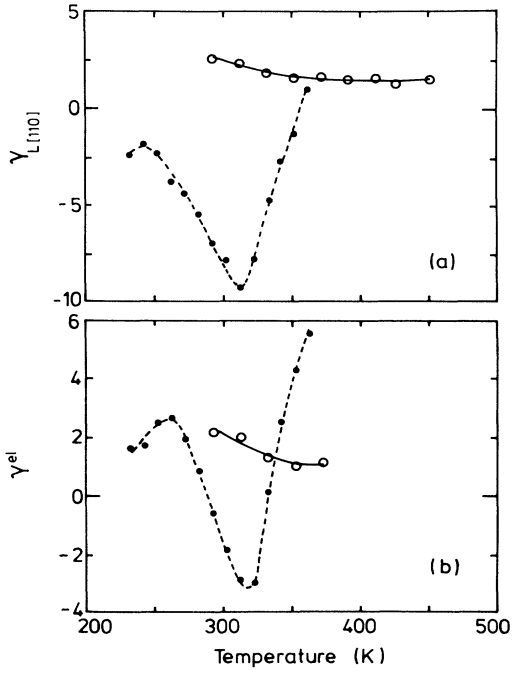

FIG. 7. The temperature dependence of (a) the long-wavelength longitudinal acoustic-mode Grüneisen parameter $\gamma_{L[110]}$ and (b) the mean acoustic Grüneisen parameter $\bar{\gamma}^{el}$ of monocrystalline $Fe_{60}Mn_{40}$ (open circles) and $Fe_{72}Pt_{28}$ (solid circles) (Ref. 15). The lines are for visual guidance.

monicities of the long-wavelength acoustic modes of $Fe_{60}Mn_{40}$ are, on average, substantially larger than those of phonons having larger wave vectors.

The Grüneisen parameters $\gamma_{L[110]}$ and $\bar{\gamma}^{el}$ of $Fe_{60}Mn_{40}$ are compared with those of $Fe_{72}Pt_{28}$ in Fig. 7. For $Fe_{60}Mn_{40}$ the longitudinal mode and the mean acoustic Grüneisen parameters are positive and decrease gradually as the material is taken up towards the Néel temperature. In the ferromagnetic phase of $Fe_{72}Pt_{28}$ the negative signs of $(\partial C_L/\partial P)_{P=0}$ and $(\partial B^S/\partial P)_{P=0}$ (Fig. 3) give rise to negative values for these acoustic Grüneisen parameters. Ultrasonic studies under pressure[14,15] have provided the first experimental evidence for negative longitudinal acoustic mode Grüneisen parameters in an Invar alloy, an observation that is directly pertinent to the Invar problem and indicate that the anomalous vibrational anharmonicity of these modes is largely responsible for negative thermal expansion of $Fe_{72}Pt_{28}$ between about 260 K and the Curie temperature.

VI. RELATIONSHIP BETWEEN THE ELASTIC AND NONLINEAR ACOUSTIC PROPERTIES AND THE INVAR BEHAVIOR OF IRON ALLOYS

A. Ferromagnetic Invar alloys: $Fe_{72}Pt_{28}$ and $Fe_{65}Ni_{35}$

A fundamental understanding of the long-standing Invar problem has only recently been achieved. The explanation stems from total-energy band calculations[17,18] for ferromagnetic alloys, using a fixed-spin-moment (FSM) procedure, which result in an energy-volume curve with a low-spin (LS) solution centered at low volume and a high-spin (HS) solution at high volume. The contribution of lattice vibrations to free energy has been included[19] by coupling the total-energy band calculations with Debye-Grüneisen theory. The energy difference $\Delta E(=E_{LS}-E_{HS})$ between the minima of the LS and HS branches is temperature dependent: ΔE decreases with increasing temperature and changes sign near room temperature. For ferromagnetic Invar alloys the HS solution defines the ground-state at low temperatures and the LS solution defines the ground state at high temperatures. The theory[17–19] explains qualitatively the essential experimental features of Invar behavior in ferromagnetic alloys including the elastic effects. The observed pause in thermal expansion (or the contraction) of ferromagnetic alloys (Fig. 1) is due to thermal population of the low-volume LS state. At low temperatures the bulk modulus is determined by the HS state and should show a moderate decrease with increasing temperature. Above the crossover temperature, the bulk modulus for the ferromagnetic Invars increases to a larger value corresponding to the low-volume, less compressible LS state. Further increase in temperature should lead to a gradual decrease in the bulk modulus. These theoretical predictions[19] are in accord with the bulk modulus measurements for Fe-Ni (Refs. 37 and 38) and $Fe_{72}Pt_{28}$ (Refs. 39 and 40) Invar alloys.

Moment instabilities are always correlated with a volume change; the coupled moment-volume fluctuations, promoted by the small energy difference ΔE, should

influence strongly the elastic and nonlinear acoustic properties of an Invar material. Application of hydrostatic pressure can be expected to enhance magnetovolume instabilities and induce large effects in the nonlinear acoustic properties of a ferromagnetic Invar, as shown by the large negative values of $(\partial C_L/\partial P)_{P=0}$ and $(\partial B/\partial P)_{P=0}$ found[14,15] for $Fe_{72}Pt_{28}$ (Fig. 3). The negative thermal expansion in the ferromagnetic phase of the Invar $Fe_{72}Pt_{28}$ (Fig. 1) is directly associated with longitudinal acoustic-mode softening (Figs. 3 and 7). At low temperatures $Fe_{72}Pt_{28}$ is in the high-volume HS state and accordingly has a small bulk modulus. At temperatures in the vicinity of the crossover temperature, application of hydrostatic pressure drives the material towards the much lower volume LS state. Hence the material tends to become more compressible as pressure is increased: this results in a negative $(\partial B/\partial P)_{P=0}$ [Fig. 3(b)]. The effect of increasing temperature is to facilitate the ease with which the HS state can be transformed to the LS state. Therefore, $(\partial B/\partial P)_{P=0}$ becomes more negative. As the temperature is increased further, the population of the LS state increases at the expense of the HS state. Above the crossover temperature but below T_c an Invar can be expected to be a composite of the HS and LS states.[17] The LS state has lower volume and is therefore less compressible than the HS state;[41] in the limit of a pure LS state the material should have a large bulk modulus with a positive $(\partial B/\partial P)_{P=0}$. Hence as a consequence of the HS to LS transition this ferromagnetic Invar should show, as found [Fig. 3(b)], a pronounced negative minimum in $(\partial B/\partial P)_{P=0}$ as a function of temperature. The very small and even negative values of $(\partial B/\partial P)_{P=0}$ found[13] for Fe-Ni at about 300 K [Fig. 3(b)] can also be accounted for on this basis.

This explanation can be put on a more formal basis as follows. The pressure derivative $(\partial B/\partial P)_T$ of the isothermal bulk modulus can be expressed by the thermodynamic relation

$$\left[\frac{\partial B}{\partial P}\right]_T = \left[\frac{\partial V}{\partial P}\right]_T \left[\frac{\partial T}{\partial V}\right]_P \left[\left[\frac{\partial B}{\partial T}\right]_P - \left[\frac{\partial B}{\partial T}\right]_V\right]. \tag{13}$$

The values of $(\partial V/\partial P)_T$, $(\partial T/\partial V)_P$, and $(\partial B/\partial T)_P$ have been estimated as a function of temperature using the results of Moruzzi.[19] The first term on the right-hand side of Eq. (13) is found to show (Fig. 8) a minimum in the middle of the temperature range where the material behaves as a composite of HS and LS states. The magnitude of this minimum also depends on the second term which could not be evaluated. These predictions of the new Invar theory[17–19] are in accord with those found experimentally for $(\partial B/\partial P)_{P=0}$ of $Fe_{72}Pt_{28}$ [Fig. 3(b)].

B. Antiferromagnetic Invar alloys: $Fe_{60}Mn_{40}$

The theoretical explanation of the source of the Invar behavior ferromagnetic alloys can be extended to antiferromagnetic alloys with the proviso that the antiferromagnetic Invar systems must be characterized by antiferro-

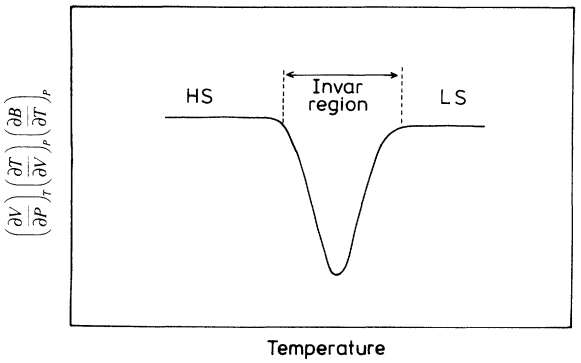

FIG. 8. The temperature dependence of the estimated value of the first term $(\partial V/\partial P)_T(\partial T/\partial V)_P(\partial B/\partial T)_P$ on the right-hand side of Eq. (13).

magnetic and nonmagnetic (NM) states and that the ferromagnetic high-spin state is replaced by an antiferromagnetic high-spin state which, at low temperatures, has a minimum at a lower energy than the NM state.[17,18] A total-energy calculation[42] for the ordered fcc Fe_2Mn_2 compound with collinear spin alignment showed that the AFM state defines the ground state for all physically relevant atomic volumes; the energy difference $\Delta E = E_{NM} - E_{AFM}$ between the minima of NM and AFM branches is only about 1 mRy (158 K); the moments of Fe atoms alone vanish while the Mn atoms retain their full moment. This instability of Fe moments in Fe_2Mn_2 takes place very close to equilibrium rigid-lattice constant; the calculated equilibrium magnetic moments are about $1.15\mu_B$ for Mn and null for Fe.[42] In practice, the fcc Fe-Mn alloys are disordered and have a noncollinear AFM ordering.[3,43] Furthermore, the experimental local moment μ_{Fe} of Fe atoms in disordered Fe-Mn alloys is different from zero and does not change appreciably with the change of the composition of Fe from 50 to 70%.[3] For fcc $Fe_{60}Mn_{40}$, μ_{Fe} decays rapidly with increasing temperature up towards T_N; however, the temperature dependence of the magnetic moment of Mn atoms shows a small decrease with increasing temperature up to about 400 K and then a sharp drop near T_N.[22,3] These results for μ_{Fe} indicate that Fe atoms in fcc Fe-Mn alloys are in an antiferromagnetic HS state at low temperatures; with increasing temperature μ_{Fe} decreases (i.e., the population of the NM state increases). In fact, above the crossover temperature, $\mu_{Fe}(T)/\mu_{Fe}(0)$ should not be zero because the system behaves as a composite of HS and NM states. Thus, a decrease in the pressure derivatives of both C_L and B^S is to be expected in the vicinity of the crossover temperature. This argument is in agreement with the experimental results obtained for $(\partial C_L/\partial P)_{P=0}$ and $(\partial B^S/\partial P)_{P=0}$ of $Fe_{60}Mn_{40}$ Invar alloy (Table II). At still higher temperatures, the application of pressure may enhance the interatomic repulsive forces in the dominating low-volume NM state, leading to an increase in $(\partial C_L/\partial P)_{P=0}$ and $(\partial B^S/\partial P)_{P=0}$. However, since the magnetovolume instability affects only some constituent atoms in $Fe_{60}Mn_{40}$, as evidenced by the neutron-diffraction experiments[22,24] and theoretical calculations,[42]

a much smaller effect can be expected (Fig. 3) in accord with the rather weak anomaly in the thermal expansion (Fig. 1). The usual decrease of the bulk modulus with increasing temperature overrides the increase due to the comparatively weak magnetovolume instability in this AFM alloy; combination of the two conflicting effects accounts for a noticeable gradient change in the temperature dependence of B^s [Fig. 2(d)] in the Invar range centered around room temperature.

VII. CONCLUSIONS

The velocities of the three ultrasonic modes propagated along the [110] direction of an antiferromagnetic fcc $Fe_{60}Mn_{40}$ single-crystal alloy have been measured as functions of temperature between 4.2 and 750 K and hydrostatic pressure up to 0.15 GPa at selected temperatures from 293 to 453 K. The data have been used to determine the temperature dependences of the independent elastic-stiffness tensor components C_{IJ} and the adiabatic bulk modulus B^S and their pressure derivatives $(\partial C_{IJ}/\partial P)_{P=0}$ and $(\partial B^S/\partial P)_{P=0}$. The physical significance of the results can be summarized as follows.

(i) The pronounced softening in the temperature dependence of the longitudinal elastic stiffness C_L, found for ferromagnetic Invars below the Curie temperature, is absent in this antiferromagnetic Invar alloy: for $Fe_{60}Mn_{40}$ C_L shows a small dip at the Néel temperature T_N (=467 K). The bulk modulus also shows a cusplike decrease around T_N.

(ii) The shear modulus C' exhibits a steplike reduction (about 3.8%) as the temperature is lowered through T_N, while C_{44} shows only a small change in gradient near this point.

(iii) The contributions of antiferromagnetic ordering to C_L, C', and B^S start at about 575 K, well above T_N, and are negative for all temperatures: in the antiferromagnetic state C_L, C', and B^S are softened, while C_{44} is stiffened slightly.

(iv) The hydrostatic pressure derivatives $(\partial C_L/\partial P)_{P=0}$ and $(\partial B^S/\partial B)_{P=0}$ decrease markedly with increasing temperature from room temperature up towards T_N.

(v) The thermal Grüneisen parameter $\gamma^{\rm th}$ is just less than unity in the temperature range below 420 K and shows a shallow minimum around room temperature; above T_N, $\gamma^{\rm th}$ increases up to a value of 2 at 600 K. These results for $\gamma^{\rm th}$ are in accord with the thermal expansion of this Invar alloy as a function of temperature. The long-wavelength longitudinal acoustic-mode Grüneisen parameter $\gamma_{L[110]}$ and the mean acoustic-mode Grüneisen parameter $\overline{\gamma}^{\rm el}$ of monocrystalline $Fe_{60}Mn_{40}$ are positive and decrease with increasing temperature. In the case of ferromagnetic $Fe_{72}Pt_{28}$, which shows much more pronounced Invar behavior in the form of negative thermal expansion, the Grüneisen parameters of the volume-dependent longitudinal acoustic modes are strongly negative in the Invar region.

(vi) The temperature dependence of the bulk modulus B^S and its hydrostatic pressure derivative $(\partial B^S/\partial P)_{P=0}$ for $Fe_{72}Pt_{28}$, which shows pronounced minima in the Invar region, can now be understood on the basis of the recently developed theory[17–19] involving a transition from the high-volume high-spin state at low temperatures to the low-volume low-spin state at high temperatures. A similar explanation is valid also for the much smaller Invar and nonlinear acoustic effects observed for the antiferromagnetic $Fe_{60}Mn_{40}$ alloy.

ACKNOWLEDGMENTS

We are grateful to the Deutsche Forschungsgemeinschaft (SFB 166) for financial support. We would also like to thank E. F. Lambson for technical assistance. One of us (M.C.) would like to acknowledge the hospitality of the School of Physics, University of Bath during his sabbatical visit.

*Permanent address: Hacettepe University, Department of Physics, Ankara, Turkey.

[1]M. Hansen, *Constitution of Binary Alloys* (McGraw-Hill, New York, 1958).
[2]H. Schumann, Arch. Eisenhüttenwesen **38**, 647 (1967).
[3]Y. Endoh and Y. Ishikawa, J. Phys. Soc. Jpn. **30**, 1614 (1971).
[4]H. Fujimori, J. Phys. Soc. Jpn. **21**, 1860 (1966).
[5]Y. Tanji, J. Jpn. Inst. Met. **35**, 1 (1971).
[6]Y. Endoh, Y. Noda, and M. Iizumi, J. Phys. Soc. Jpn. **50**, 469 (1981).
[7]W. Stamm, Ph.D. thesis, University of Duisburg, 1988.
[8]E. F. Wassermann, in *Ferromagnetic Materials,* edited by K. H. J. Buschow and E. P. Wohlfarth (North-Holland, Amsterdam, 1990), Vol. V, p. 237.
[9]F. Richter and W. Pepperhoff, Arch. Eisenhüttenwesen **47**, 45 (1976).
[10]E. F. Wassermann, M. Acet, and W. Pepperhoff, J. Magn. Magn. Mater. **90&91**, 126 (1990).
[11]E. F. Wassermann, J. Magn. Magn. Mater. **100**, 346 (1991).
[12]J. T. Lenkkeri, J. Phys. F **11**, 1991 (1981).
[13]Ph. Renaud, Ph.D thesis, Université de Lausanne, Switzerland, 1988.
[14]Ll. Mañosa, G. A. Saunders, H. Rahdi, U. Kawald, J. Pelzl, and H. Bach, J. Phys. Condens. Matter **3**, 2273 (1991).
[15]Ll. Mañosa, G. A. Saunders, H. Rahdi, U. Kawald, J. Pelzl, and H. Bach, Phys. Rev. B **45**, 2224 (1992).
[16]K. Sumiyama, M. Shiga, M. Morioka, and Y. Nakamura, J. Phys. F **9**, 1665 (1979).
[17]V. L. Moruzzi, Physica B **161**, 99 (1989).
[18]V. L. Moruzzi, Phys. Rev. B **41**, 6939 (1990).
[19]V. L. Moruzzi, Solid State Commun. **83**, 739 (1992).
[20]H. Bach, S. Erdt, and P. Stauche, J. Cryst. Growth **62**, 173 (1983).
[21]W. Bendick and W. Pepperhoff, J. Phys. F **8**, 2535 (1978).
[22]Y. Ishikawa and Y. Endoh, J. Phys. Soc. Jpn. **23**, 205 (1967).
[23]E. P. Papadakis, J. Acoust. Soc. Am. **42**, 1045 (1967).

[24]S. C. Flower and G. A. Saunders, Philos. Mag. B **62**, 311 (1990).
[25]R. N. Thurston and K. Brugger, Phys. Rev. **133**, A1604 (1964).
[26]D. P. Dandekar, J. Appl. Phys. **41**, 667 (1970).
[27]R. F. S. Hearmon, in *Elastic, Piezoelectric, Pyroelectric, Piezooptic, Electrooptic Constants and Nonlinear Dielectric Susceptibilities of Crystals,* edited by K.-H. Hellwege, Londolt-Bornstein, New Series, Vol. 11 (Springer-Verlag, Berlin, 1979), p. 11.
[28]J. T. Lenkkeri, J. Phys. F **11**, 1997 (1981).
[29]G. Hausch and E. Török, J. Magn. Magn. Mater. **6**, 269 (1977).
[30]S. C. Lakkad, J. Appl. Phys. **42**, 4277 (1971).
[31]T. Hashimoto and Y. Ishikawa, J. Phys. Soc. Jpn. **23**, 213 (1967).
[32]R. D. Lowde, R. T. Harley, G. A. Saunders, M. Sato, R. Scherm, and C. Underhill, Proc. R. Soc. London, Ser. A **374**, 87 (1981).
[33]U. Kawald, W. Zemke, H. Bach, J. Pelzl, and G. A. Saunders, Physica B **161**, 72 (1989).
[34]O. L. Anderson, J. Phys. Chem. Solids **27**, 547 (1966).
[35]W. C. Overton, J. Chem. Phys. **37**, 116 (1962).
[36]K. Brugger, Phys. Rev. **157**, 524 (1967).
[37]Ph. Renaud and S. G. Steinemann, Physica B **161**, 75 (1989).
[38]M. Shiga, K. Makita, K. Uematsu, Y. Muraoka, and Y. Nakamura, J. Phys. Condens. Matter **2**, 1239 (1990).
[39]G. Hausch, J. Phys. Soc. Jpn. **37**, 819 (1974).
[40]G. Oomi and N. Mori, J. Phys. Soc. Jpn. **50**, 2917 (1981).
[41]G. A. Saunders, Wang Qingxian, E. F. Lambson, N. Lodge, D. Paine, and W. Hönle, J. Phys. Condens. Matter **2**, 3713 (1990).
[42]M. Podgorny, Phys. Rev. B **45**, 797 (1992).
[43]S. Kawarazaki, Y. Sasaki, K. Yasuda, T. Mizusaki, and A. Hirai, J. Phys. Condens. Matter **2**, 5747 (1990).
[44]H. Umebayashi and Y. Ishikawa, J. Phys. Soc. Jpn. **21**, 1281 (1966).